© 2002 Oxford University Press Human Molecular Genetics, 2002, Vol. 11, No. 16 1887–1898

Mutation of the novel gene *Tmie* results in sensory cell defects in the inner ear of spinner, a mouse model of human hearing loss DFNB6

Kristina L. Mitchem[1], Ellen Hibbard[1], Lisa A. Beyer[1], Ken Bosom[3], Gary A. Dootz[1], David F. Dolan[1], Kenneth R. Johnson[3], Yehoash Raphael[1] and David C. Kohrman[1,2,*]

[1]Department of Otolaryngology/Kresge Hearing Research Institute and [2]Department of Human Genetics, University of Michigan Medical School, Ann Arbor, Michigan 48109, USA and [3]The Jackson Laboratory, Bar Harbor, Maine 04609, USA

Received April 22, 2002; Revised and Accepted June 7, 2002 DDBJ/EMBL accession nos.[†]

The recessive mutation at the mouse spinner (*sr*) locus results in hearing loss and vestibular dysfunction due to neuroepithelial defects in the inner ear. Using a positional cloning strategy, we have identified the mutant locus responsible for this pathology. The affected gene (*Tmie*) lies within a 40 kb deletion in the original *sr* allele. In a newly identified allele, *Tmie* contains a nonsense mutation expected to truncate the C-terminal end of its product. The 153 amino acid protein encoded by the gene shows no similarity to other known proteins, and is predicted to contain a signal peptide and at least one transmembrane domain. *Tmie* transcripts were identified in several tissues, including the cochlea. Loss of function of *Tmie* results in postnatal alterations of sensory hair cells in the cochlea, including defects in stereocilia, the apical projections of hair cells that are important in mechanotransduction of sound. These morphological defects are associated with a profound failure to develop normal auditory function. Consistent with a conserved role for this gene in the cochlea, the genetic mapping data presented here support human *TMIE* as the gene affected at DFNB6, a non-syndromic hearing loss locus. The spinner mutant is thus a valuable model for insight into mechanisms of human deafness and development of sensory cell function.

INTRODUCTION

The incidence of hearing loss in humans is substantial, with a frequency of prelingual deafness as high as 0.1–0.2%, and a similar frequency of postlingual deafness before the third decade of life (1,2). In developed nations, ~50% of these cases appear to have a genetic basis (1). Inherited deafness in humans is genetically heterogeneous, with effects in any one of more than 100 distinct genes likely to be responsible for non-syndromic hearing loss (1). Despite the difficulties in analysis of genetically heterogeneous conditions, there has been dramatic progress in the localization and identification of a large number of genes associated with hearing loss during the past several years (3–5). Mouse genetic models provide a valuable approach to identify genes which play a role in inherited human hearing loss, and also offer a useful system in which to investigate gene function (6). Identification and analysis of these genes in the mouse has implicated a diverse array of proteins required in the inner ear during early embryonic development and postnatal maturation of the sensory neuroepithelium, and in the adult organ (7).

The spinner (*sr*) mutation arose spontaneously over 40 years ago in a colony of C57BL mice and was first recognized by behavioral dysfunction, including bidirectional circling and head shaking (8). Auditory function in spinner mice was found to be reduced, based upon the lack of a startle reflex to sound at any age. Breeding experiments indicated that these defects were inherited in an autosomal recessive fashion. Low-resolution linkage studies localized *sr* to distal chromosome 9, with respect to genes encoding two catalytic enzymes, mannose phosphate isomerase 1 (*Mpi1*) and cytosolic malate dehydrogenase (*Mod1*) (9). Comparative gene mapping studies have identified a region of conserved synteny between distal chromosome 9 in the mouse and chromosome 3 in humans (10). Analysis of an Indian family with members exhibiting autosomal recessive non-syndromic hearing loss indicated the

*To whom correspondence should be addressed at: University of Michigan Medical School, Department of Otolaryngology/Kresge Hearing Research Institute, 9301D MSRB III, 1150 West Medical Center Drive, Ann Arbor, MI 48109-0648, USA. Tel: +1 7347639653; Fax: +1 7346472563; Email: dkohrman@umich.edu

[†]AF481144, AF481143 and AF481142

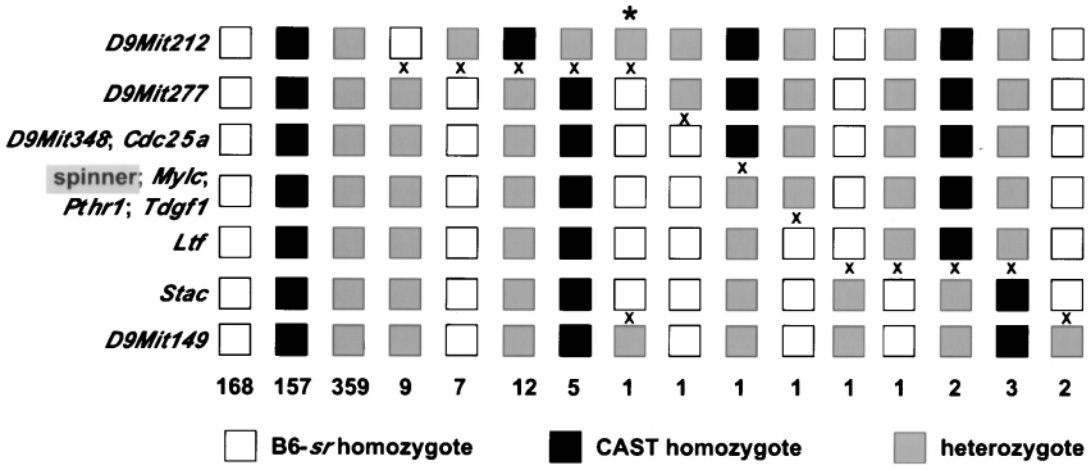

Figure 1. Localization of the *sr* locus on distal chromosome 9. The allele distribution patterns (ADP) of 730 F2 offspring of a (C57BL/6J-*sr* × CAST) F1 intercross are shown. Locus order was determined by minimizing the total number of crossovers across this 3 cM region. '×' indicates the inferred positions of recombination events. Numbers of F2 mice exhibiting the corresponding ADP are noted. The asterisk indicates an F2 mouse that inherited single recombinant chromosomes from each F1 parent.

presence of a deafness locus (DFNB6) on the short arm of chromosome 3 (11). Hearing loss in affected family members was present at birth and was severe to profound across all tested frequencies. Haplotype analysis indicated that DFNB6 was localized in a 14–20 cM region, within 3p21–3p14. The conserved synteny of this region suggested that spinner may be a molecular model for DFNB6.

Light microscopic examination of the inner ears of affected spinner mice indicated that auditory and vestibular dysfunction were likely to be peripheral in origin (8). No obvious defects in gross inner ear morphogenesis or neuroepithelial cell patterning were noted. Sensory cells in the cochlea, however, were decreased slightly in size by postnatal day (P) 15, and were completely degenerated by P40. Later defects were also noted, including degeneration of auditory nerve cells. Vestibular pathology appeared to be restricted to the macula of the sacculus, where progressive loss of sensory hair cells also occurred. These specific defects, along with the apparent lack of affected tissues outside of the inner ear, indicated that spinner belonged to the neuroepithelial class of mouse deafness mutants (12). In the current study, we have used a positional cloning approach to identify mutations in a novel gene as the basis for the spinner phenotype. We have also identified postnatal defects in sensory cell ultrastructure that are associated with profound hearing loss in affected spinner mice.

RESULTS

Previous linkage studies indicated that *sr* is located on chromosome 9, ~20 cM distal of *Mod1* (9). In order to localize the mutation with greater resolution, we generated an inter-subspecific intercross between (C57BL/6J-*sr* × CAST/Ei) F1 mice. The percentage of affected mice obtained (180/730, 24.7%) was consistent with previous segregation data indicating recessive inheritance of behavioral and auditory defects (8). Analysis of genotypes from the 730 F2 progeny indicated that *sr* lies within a 0.2 cM interval between D9Mit348 and *Ltf* (Fig. 1). Gene localization on this map placed the *sr* locus within a previously identified region of conserved synteny with human chromosome 3 (Fig. 2) (10). *Cdc25a* was localized proximal of *sr*, while parathyroid hormone receptor 1 (*Pthr1*), myosin light chain (*Mylc*) and teratocarcinoma-derived growth factor 1 (*Tdgf1*) were non-recombinant with the *sr* locus. The human orthologs of these four genes were previously localized to 3p21–22 (13–16). *Stac* was localized 0.6 cM distal of *sr*; human *STAC* was previously mapped to 3p22.3 (17). As relative gene order appears to be well conserved across the region in mouse and human (Fig. 2), the likely location of the human ortholog of the spinner gene is therefore 3p21–22, closely linked to *MYL3* and *PTHR1*. Based upon recent assembly of human genomic sequence, this location lies within the DFNB6 candidate region, and is consistent with the gene as a positional candidate for the affected locus, as previously suggested (11).

Using closely linked markers, we identified a large collection of BAC genomic clones across the spinner candidate region on mouse chromosome 9 (Fig. 3). While assessing BAC clone overlap, we found that several markers were deleted from genomic DNA of *sr/sr* mice (Fig. 3). Through bioinformatics analysis of available genomic sequences, we identified four genes in the immediate region. *AK007173* and *Tsp50* encode proteins with strong similarity to serine-type proteases. *mRn.49018*, a gene with high sequence similarity to a predicted rat gene, encodes a protein with a Dbl homology domain. Dbl domains are present in guanine nucleotide exchange factors specific for Rho-family GTPases (18). *Mm.87012* is a gene with no significant similarity to other database sequences.

We confirmed the extent and structure of the deletion by Southern blot and PCR analysis. Probes derived from DNA flanking the deleted region hybridized to *Bgl*II restriction fragments of 2.1 kb and 5.2 kb in normal C57BL/6J DNA (probes I and III; Fig. 4B). In *sr/sr* DNA, both probes instead hybridized to a common-sized junction fragment of 5.8 kb, consistent with deletion of the intervening DNA. A probe

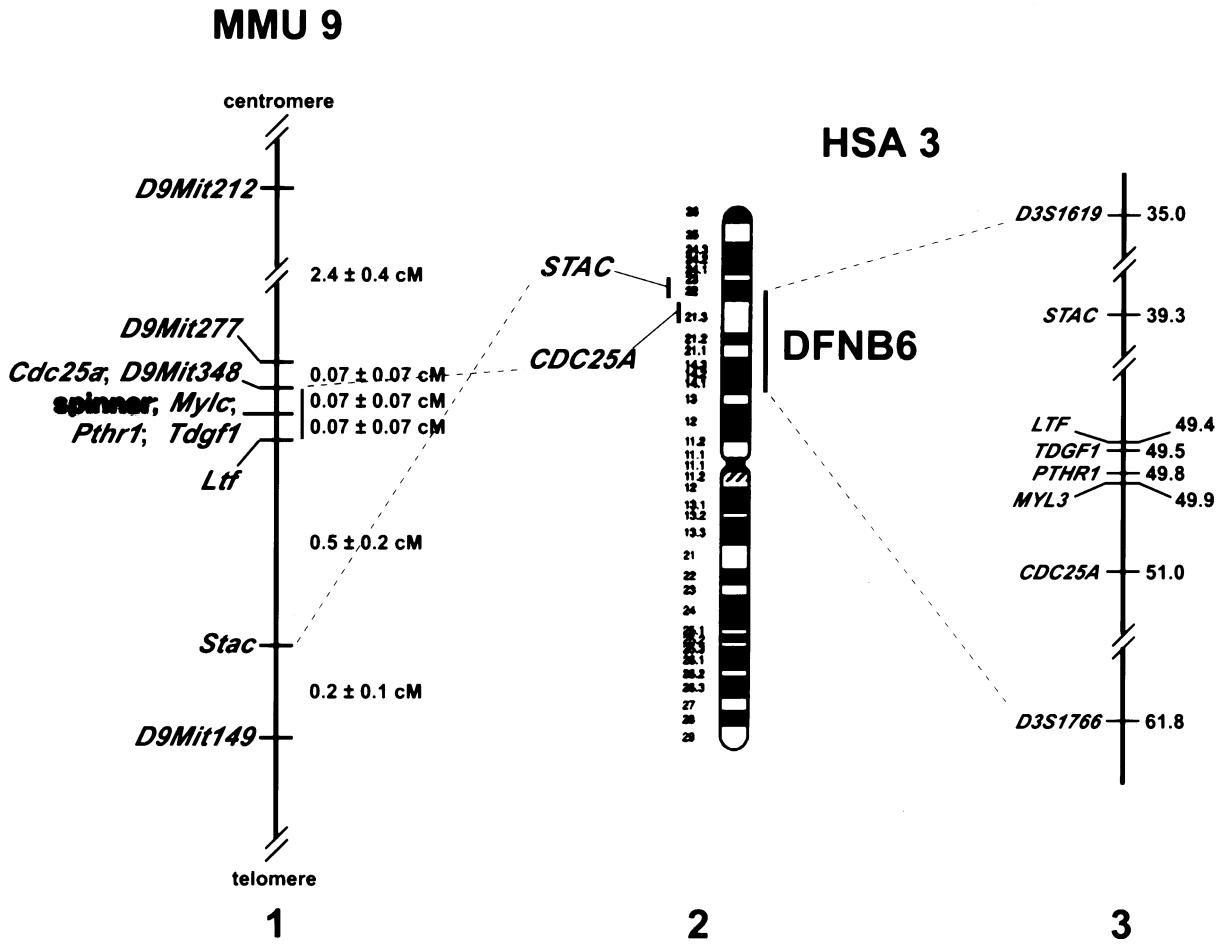

Figure 2. The human ortholog of the spinner gene is a positional candidate for the gene affected at the DFNB6 locus. The genetic map (map 1) is based on linkage analysis of the (C57BL/6J-*sr* × CAST) F1 intercross. The spinner locus lies between *D9Mit348*/*Cdc25a* and *Ltf* (vertical bar), within a non-recombinant region ≤0.2 cM in size (95% confidence interval). Distances between markers are indicated (± SE). Gene localization on this map placed the *sr* locus within a previously identified region of conserved synteny with human chromosome 3 (10). *Cdc25a* and *Stac* were localized proximal and distal, respectively, of the spinner candidate region. The human orthologs of these genes (*CDC25A* and *STAC*) have been localized to the 3p21–24 region in humans (map 2) (14,17). Linkage data indicated that the DFNB6 locus lies between markers *D3S1619* and *D3S1766* on human 3p (11). Based upon assembly of human genome sequences, gene order is well conserved between mouse and human across this region (NCBI Build 28; map 3). The spinner orthologous region is located within the DFNB6 candidate region, consistent with spinner as a molecular model of DFNB6. Numbers on the right indicate distance from the 3p telomere, in Mb.

derived from the 3′-UTR of *Mm.87012* (probe II) hybridized with 1.1 kb fragments of DNA from C57BL/6J and +/*sr*, but failed to hybridize with DNA from *sr/sr*, consistent with deletion of this probe region. Primer pairs designed from sequences flanking the centromeric breakpoint (primers 1 + 2) and the telomeric breakpoint (primers 3 + 4) of the deletion amplified products of the predicted size from C57BL/6J and +/*sr* DNA but not from *sr/sr* DNA (Fig. 4C). Primers flanking the deletion (primers 1 and 4) amplified an *sr*-specific product only, again consistent with a deletion. The deletion, as assayed using these primer sets, showed absolute co-segregation with the *sr* locus in the genetic cross (unpublished data). Sequence analysis of the amplification products indicated that the deletion breakpoints occurred within direct repeats of the sequence CTCAG (Fig. 4D). These repeats are separated by ∼40 kb in the normal C57BL/6J chromosome, based upon genomic sequence comparisons. The centromeric deletion breakpoint is within *AK007173* (Fig. 4A); the 3′ end of the gene is deleted. *Tsp50* and *Mm.87012* lie completely within the deletion. The telomeric deletion breakpoint is within *mRn.49018*; the spinner deletion removes the 5′ end of the gene. Despite the complete or partial loss of these four genes, affected spinner mice exhibit no obvious phenotypic defects other than inner ear dysfunction.

We recently identified a new vestibular mutant that arose spontaneously on the BXA-4 recombinant inbred strain. Like spinner, the new mutant exhibited circling and head-shaking behaviors, and a defective startle response indicative of hearing loss. These defects were inherited in a recessive manner. Analysis of pooled DNA of affected F2 mice from a small CAST/Ei intercross indicated linkage to microsatellite markers on distal chromosome 9. Analysis of 56 individual F2 mice demonstrated the following order: cen—D9Mit111—5.8 ± 1.6 cM—D9Mit78—1.3 ± 0.8 cM—mutation—0.9 ± 0.6 cM—D9Mit17—tel. This map position suggested potential allelism with the spinner locus. A complementation

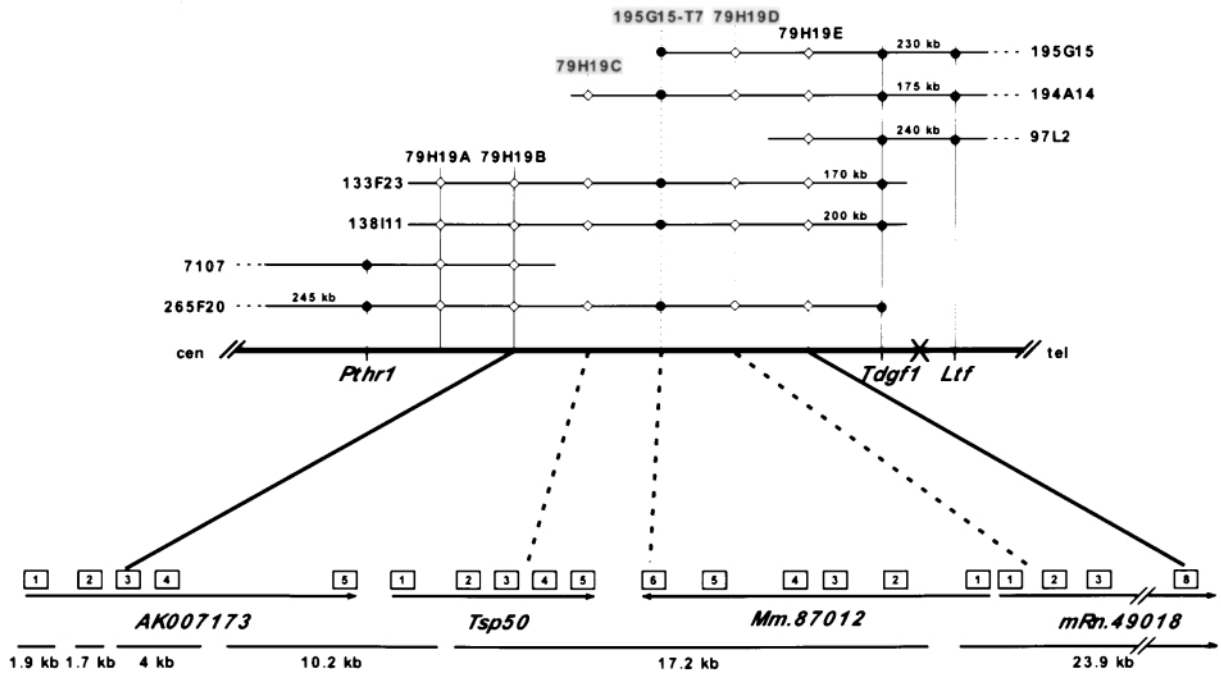

Figure 3. A genomic deletion on chromosome 9 in spinner mice. BAC clones spanning a portion of the spinner candidate region are shown at the top. The '×' on the physical map indicates the telomeric recombination breakpoint between *Tdgf1* and *Ltf*. The genetically defined candidate region for spinner is centromeric of this breakpoint. Markers present in BAC clones are indicated, as determined by hybridization (filled circles) or PCR (diamonds). The markers shaded in gray were found to be deleted from *sr/sr* genomic DNA. The gene content of the deleted region is shown below, with boxes indicating the relative positions of a subset of the exons of four genes. Sizes indicate the length of individual sequence contigs. Orientation of the sequence contigs was determined by sequence-tagged site (STS) content data of the BACs. The predicted transcriptional orientation of each gene is indicated by an arrow.

test was carried out by crossing an affected male homozygote with a female heterozygous for the original *sr* allele. Seven of 13 progeny exhibited circling behavior and lacked startle responses, consistent with allelism of the two mutations. We therefore named the new mutant sr^J.

Given the evidence for allelic mutations, we analyzed in sr^J mice the four genes affected by the deletion in the original *sr* allele. RT–PCR amplification from brain RNA with gene-specific primers indicated that all four genes were expressed in sr^J/sr^J homozygotes, with no detectable differences in transcript abundance or structure relative to C57BL/6J controls (unpublished data). RT–PCR products spanning the open reading frames of each of the four genes were then sequenced. The sequences in sr^J of *AK007173*, *Tsp50* and *mRn.49018* were identical to those in C57BL/6J controls. The only variant identified was the single nucleotide substitution C1451T in exon 5 of *Mm.87012*. This substitution was confirmed in genomic DNA from sr^J/sr^J homozygotes (Fig. 5). The sequence variant alters an arginine codon in the normal transcript to a stop codon in sr^J, truncating the predicted protein. We sequenced the corresponding region in the BXA-4 progenitor strain, eight C57BL-related strains and the A/J strain, and observed the C(1451) nucleotide in each case (Fig. 5, and unpublished data). The nonsense mutation in sr^J and the deletion in the original spinner allele indicate that defects in the *Mm.87012* gene are responsible for the spinner phenotype.

Assembly of overlapping cDNA and RT–PCR sequences of *Mm.87012* identified a transcript of 2.6 kb. Comparison of cDNA and genomic sequences indicated that the gene is composed of six exons, encompassing ~14 kb of genomic DNA (Fig. 6A). A 459 bp open reading frame spans exons three to six and encodes a 153 amino acid protein (Fig. 6B). The amino acid sequence exhibits no significant similarity to any known protein. Two hydrophobic transmembrane (TM) domains were predicted near the N-terminus by pattern recognition algorithms, with one TM domain overlapping a strongly predicted signal peptide at the extreme N-terminus. Following cleavage of the signal peptide and retention of the protein in the membrane via the second TM domain, the mature N-terminus is expected to be extracellular (or lumenal) and the C-terminus cytoplasmic (19). The C-terminal region of the protein is rich in charged residues (36/74), and includes two clusters of lysine residues. The nonsense mutation identified in sr^J mice is expected to truncate the protein at amino acid 96 and prevent expression of the majority of the C-terminal charged domain.

Northern analysis with a probe derived from the 3′ UTR of *Mm.87012* demonstrated expression of the gene in brain, kidney, liver and lung (Fig. 7A). Kidney expressed two transcripts, 2.8 and 3.2 kb in size. Brain expressed a smaller 2.2 kb transcript, while liver and lung expressed only the larger 3.2 kb transcript. Preliminary evidence suggests that the various transcript sizes derive from the use of alternative promoters and 5′ non-coding exons in the different tissues (unpublished data). Expression of the gene was also detected in cochlear RNA by RT–PCR (Fig. 7B). Based upon the predicted transmembrane domains, and its critical requirement in the inner ear, we have renamed this gene *Tmie*, for transmembrane inner ear.

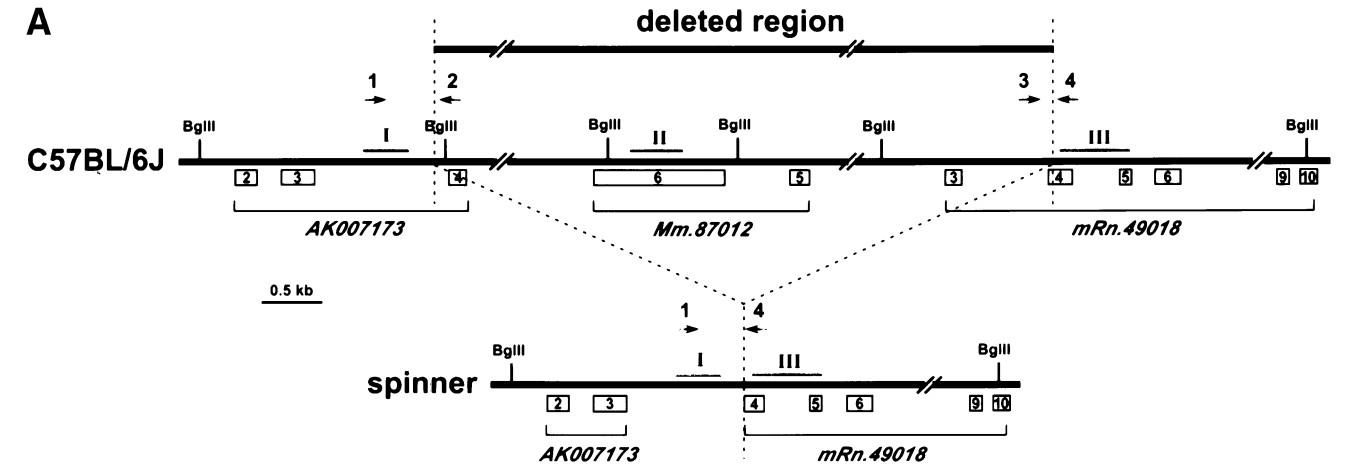

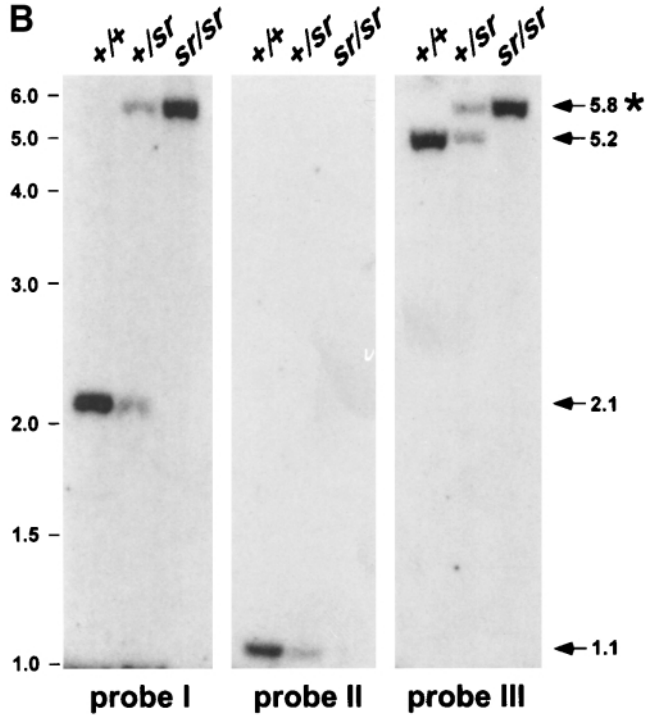

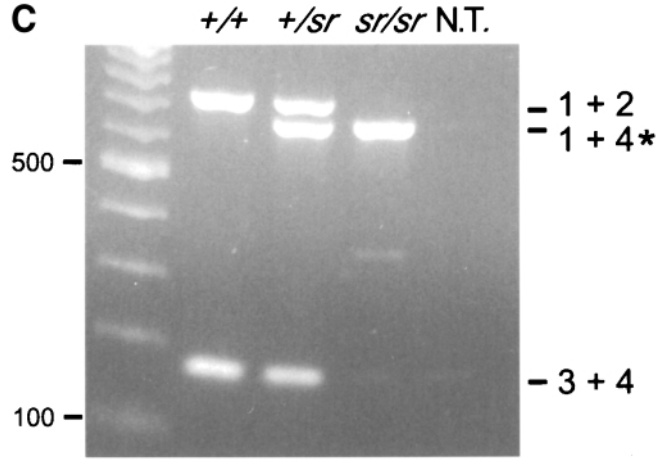



Figure 4. Confirmation of the genomic deletion and identification of deletion breakpoints. (**A**) Diagram of the deleted region, showing the positions of *Bgl*II sites and partial genomic structures of three of the four genes directly affected by the deletion. The positions of the hybridization probes (gray bars) used in (B) and the primers (arrows) used in (C) are indicated. (**B**) Three identical Southern blots of *Bgl*II-digested genomic DNA from C57BL/6J (+/+), C57BL/6J-+/*sr* (+/*sr*), and C57BL/6J-*sr/sr* (*sr/sr*) were hybridized with probes derived from the centromeric (probe I) or telomeric (probe III) side of the deletion, or from within the deleted region (probe II). Probes I and III hybridized to a common 5.8 kb junction fragment (asterisk) in *sr/sr* DNA, while probe II failed to hybridize to *sr/sr* DNA, consistent with deletion of the intervening DNA. Sizes of molecular standards are indicated on the left, in kb. Sizes of hybridizing fragments are indicated on the right, in kb. (**C**) Primer pairs designed from sequences flanking the centromeric (primers 1 + 2) and telomeric (primers 3 + 4) breakpoints of the deletion, and primers 1 + 4, were used separately to amplify each genomic template. Equivalent amounts of each PCR reaction derived from common templates were pooled and electrophoresed together in the same lanes of a 1.5% agarose gel. The expected centromeric (750 bp) and telomeric (180 bp) products were amplified from +/+ and +/*sr* DNA, but not from *sr/sr* DNA. Primers 1 and 4 amplified an *sr*-specific 660 bp product (asterisk), consistent with deletion of the intervening DNA. Sizes of molecular standards are indicated on the left, in bp. NT, no template. (**D**) Products amplified from +/*sr* were purified and sequenced. Sequence identity between the centromeric flank (primer set 1+2) and the *sr/sr* product (primer set 1 + 4), and between the telomeric flank (primer set 3 + 4) and the *sr/sr* product, indicated that the deletion breakpoints occurred within direct repeats of the sequence CTCAG (gray box).

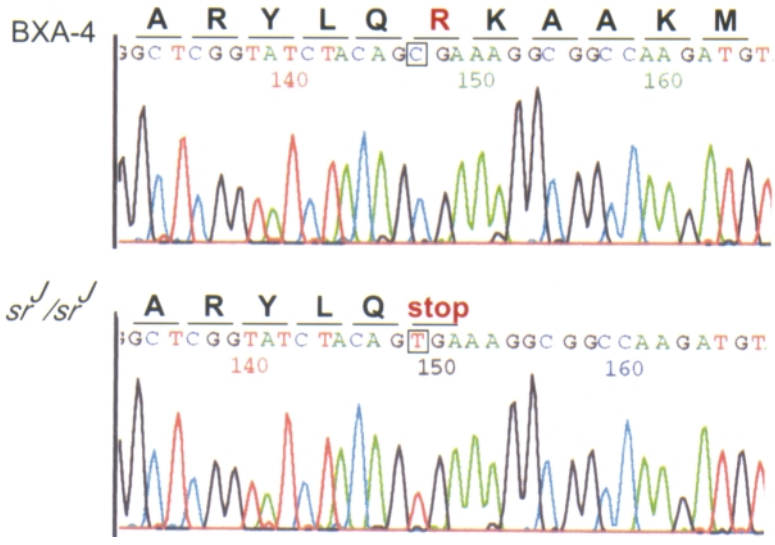

Figure 5. A single base pair substitution within exon 5 of the *Mm.87012* gene in sr^J. Sequence traces from exon 5 of the *Mm.87012* gene from BXA-4 (top) and sr^J/sr^J (bottom). A C(1451)T transition that introduces a TGA stop codon in place of an arginine codon was identified in sr^J. This nonsense mutation is expected to truncate the normal 153 amino acid product of this gene to 96 amino acid.

Control +/*sr* mice detected external sound stimuli at P14 as assessed by auditory brainstem response analysis, while *sr/sr* mice failed to exhibit responses at this age (Fig. 8) or at later time points (unpublished data). Homozygous sr^J mice also exhibited a complete lack of evoked brainstem responses (unpublished data). We examined cochlear ultrastructure in *sr* mutants to determine whether this early functional loss was correlated with morphological defects. General neuroepithelial cell patterning was normal in the cochlea of control +/*sr* (Fig. 9A) and *sr/sr* (Fig. 9B) mice at P15. Closer examination, however, revealed irregularities at the apical surfaces of both inner sensory hair cells (IHCs) and outer sensory hair cells (OHCs) in *sr/sr* (Fig. 9B). Compared to those of +/*sr* controls (Fig. 9C), IHCs of *sr/sr* mice exhibited extra rows of maturing stereocilia (Fig. 9D). Deflection of stereocilia plays a fundamental role in the mechanotransduction of sound energy by hair cells, through physical gating of a putative cation channel in the plasma membrane surrounding the actin-rich core of the stereocilia (20). IHCs of *sr/sr* mice also retained their kinocilia, suggesting a block or delay in maturation (Fig. 9D). IHCs of the controls have lost this transient, microtubule-containing structure, consistent with previous developmental studies (21). On OHCs, individual stereocilia appeared irregular in *sr/sr*, with portions of each bundle missing or considerably shortened (Fig. 9F). The apical surface areas of *sr/sr* OHCs (Fig. 9F) were also decreased compared to normal OHCs (Fig. 9E), consistent with original light microscopic studies of spinner (8). The surface areas of supporting cells that surround OHCs in *sr/sr* were correspondingly increased. We identified indistinguishable pathologies in the cochleae of sr^J/sr^J mice (unpublished data), indicating that deletion of three additional genes in the original *sr* allele does not apparently contribute to the inner ear phenotype of the mutant. These defects suggest a critical requirement for *Tmie* function during postnatal maturation of the neuroepithelium.

DISCUSSION

The current study provides strong evidence that defects in *Tmie* are responsible for inner ear dysfunction in the spinner mutant. First, this gene is localized within the small candidate interval defined by high-resolution genetic analysis. Second, mutations were identified in two independent alleles of spinner. The entire *Tmie* gene is deleted in the original *sr* allele, while in the sr^J allele, the gene contains a single base pair substitution that truncates the expected protein product. Both mutations result in profound loss of auditory function. Our genetic mapping data support the human ortholog of *Tmie* as an excellent positional candidate for the gene affected at the DFNB6 locus. Indeed, mutations have recently been identified in *TMIE* in each of five pedigrees segregating hearing loss due to defects at this locus, implicating *TMIE* as a critical gene in the human inner ear (22). The human mutations include a small deletion and an insertion that alter the normal open reading frame and that are likely to be complete loss-of-function alleles. Finally, *Tmie* is expressed in the cochlea, consistent with the specific inner ear pathology identified in affected spinner mice.

The postnatal defects present in the cochleae of *sr/sr* mice suggest a requirement for *Tmie* during maturation of sensory cells, including the normal development or maintenance of stereocilia bundles. A number of other genes have been implicated in pathways critical for normal stereocilia structure, including those which encode unconventional myosins [*Myo7a* (23), *Myo6* (24), and *Myo15* (25)], members of the cadherin superfamily [*Cdh23* (26) and *Pcdh15* (27–29)], an integrin subunit [*Itga8* (30)], and an actin-bundling protein [*Espn* (31)]. Based upon specific bundle defects in deaf mice carrying mutations in these genes, they appear to regulate pathways in sensory hair cells that are critical for growth, integrity or organization of the bundle. The severe shortening of individual OHC stereocilia in *sr/sr* mice suggests that the TMIE protein

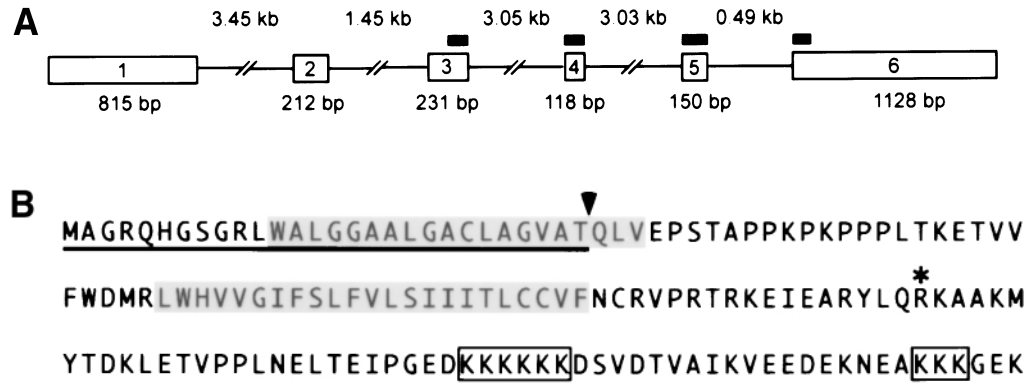

Figure 6. *Tmie* encodes a potential integral membrane protein. (**A**) The exon structure of *Tmie* is indicated, with the 459 bp open reading frame denoted by gray bars. The predicted Met start codon lies within an adequate translation initiation context (gagaacATG*g*), and is preceded by an in-frame stop codon (51). Exon–intron boundary sequences correspond to standard splicing consensus signals (unpublished data). (**B**) The predicted sequence of the TMIE protein is indicated with one-letter amino acid abbreviations. A predicted signal sequence at the N-terminus is underlined; the predicted cleavage site is indicated by an arrow. Two potential transmembrane domains are indicated by gray boxes. Two regions of clustered lysine residues in the C-terminus are boxed. The position of the nonsense mutation identified in the sr^{J} allele is marked by an asterisk.

may influence actin filament dynamics in the normal maturing bundle, a process also thought to be affected by MYO15 (32) and ESPN (31). The shortened stereocilia may alternatively reflect a secondary degenerative response to the mutation. Additional studies of earlier developmental time points will help to distinguish between these possibilities. The apparent delay in maturation of IHCs in *sr/sr* mice appears more subtle than the stereocilia defects found on OHCs. Given that IHC signaling provides the majority of afferent input to the central auditory system (33), the failure of the mutants to develop measurable auditory brainstem responses suggests that IHC function is severely compromised. Although we have not identified any early postnatal defects in auditory nerve morphology (unpublished data), *Tmie* mutations could also affect brainstem responses through more direct action within auditory neurons. *Tmie* thus may serve multiple roles during sensory cell development, including critical functions in both stereocilia bundle maturation and sensory transduction in IHCs or in auditory neurons. Alternatively, *Tmie* may have only a single role, and the different morphological defects in IHCs and OHCs of *sr/sr* mice may reflect cell type-specific, secondary responses to the mutation. Electrophysiological evaluation of hair cells in spinner mice should provide important information regarding a role for *Tmie* in transduction.

Tmie joins an expanding set of genes, mutations of which lead to defects in development and homeostasis in the inner ear and cause hearing loss and vestibular dysfunction (34). Based upon sequence similarities and direct biochemical studies, many of these genes belong to recognized families. Others, such as *Tmie*, exhibit little or no similarity to known genes, and their functions are presently unclear. Recently, mutations that cause human hearing loss have been identified in two other novel genes that encode potential integral membrane proteins. *USH3A* mutations are responsible for hearing loss and retinal degeneration in a subset of individuals with Usher's syndrome (35). *USH3A* encodes a small, novel protein with a signal peptide/transmembrane domain structure like that of TMIE (35). Mutations in *TMC1* are the basis for non-syndromic hearing loss in individuals with defects at the DFNA36/DFNB7/DFNB11 locus (36). Likewise, defects in *Tmc1* are responsible for inner ear dysfunction in the mouse mutants known as deafness and Beethoven (36,37). Like TMIE and USH3A, the predicted integral membrane product of *TMC1/Tmc1* has no significant similarities to other database sequences. Its predicted membrane topology (at least six transmembrane domains) and hair cell expression pattern have suggested a potential role for TMC1 as a sensory cell-specific ion channel (36).

While the predicted structure of TMIE is not consistent with a typical channel or receptor, the protein may play some other role in a cellular membrane location. TMIE may reside within an internal membrane compartment and function in pathways such as those involved in protein and/or vesicle trafficking. Alternatively, the mature protein may be localized in the plasma membrane and serve as a site of interaction for other molecules through its highly charged C-terminal domain. The multiple clusters of positively charged residues present in the C-terminus are also found in the cytoplasmic regions of a diverse set of integral membrane proteins that are linked to the cortical actin cytoskeleton through interactions with members of the ERM (ezrin, radixin, moesin) protein family (38). Mutations of these clusters to uncharged residues in the Na–H exchanger NHE1 (39) and in other membrane proteins such as CD44, CD43 and ICAM-2 (40) inhibit ERM protein binding and co-localization at membrane sites associated with actin-rich structures, including microvilli and lamellipodia. In the case of NHE-1, the abundance of these structures appeared to decrease in cells expressing the mutant proteins, consistent with a critical role of the ERM–membrane protein complexes in regulating cytoskeleton–membrane interactions (39). Positively charged residues in the C-terminus of TMIE are likely to be important in protein function, as each of three missense mutations detected in DFNB6 pedigrees replaces a different conserved lysine residue with an uncharged amino acid (22). A role for TMIE in organizing cytoskeleton–membrane interactions in sensory hair cells would be consistent

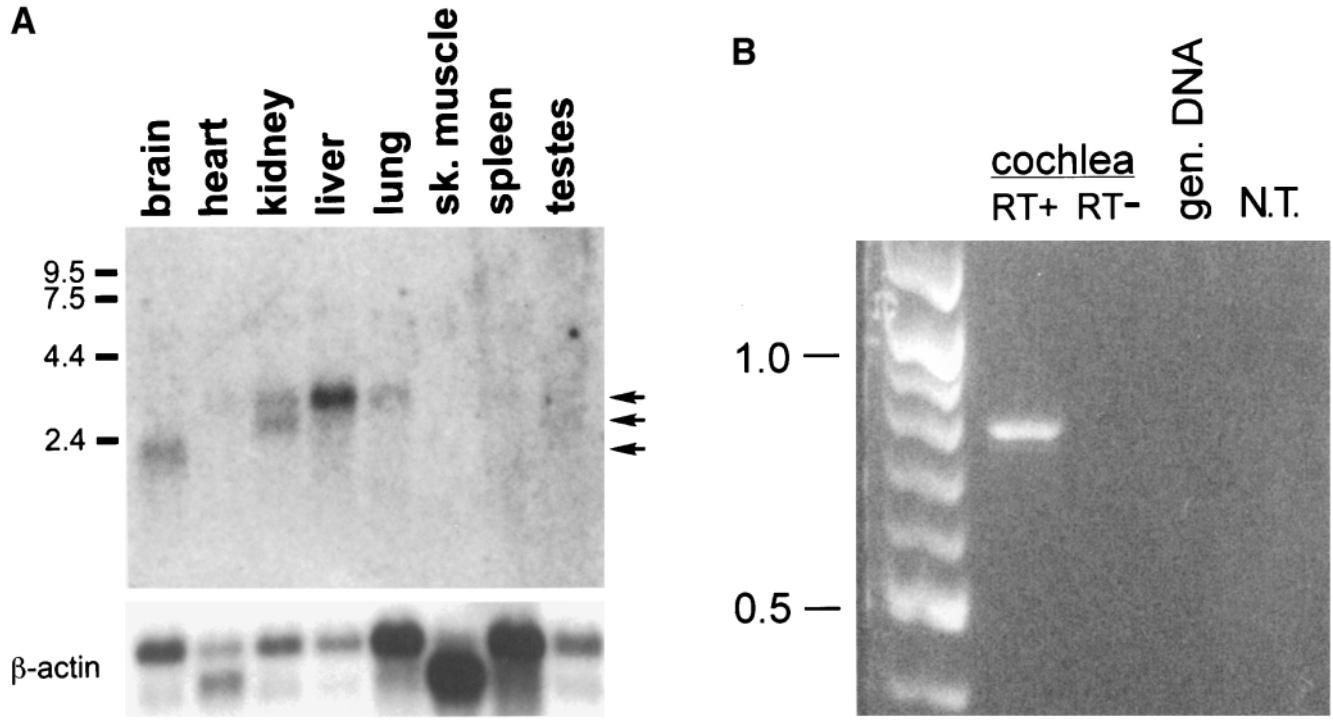

Figure 7. *Tmie* is expressed in several tissues, including the cochlea. (**A**) A northern blot containing poly(A)$^+$ RNA from multiple tissues of an adult mouse was hybridized with a probe derived from the 3′-UTR of *Tmie.* Arrows indicate the positions of the 2.2, 2.8 and 3.2 kb transcripts that were detected. The bottom panel depicts hybridization of a β-actin probe to the same blot after removal of the *Tmie* probe. Sizes of RNA molecular standards are indicated on the left, in kb. (**B**) Primers designed from exons 3 and 6 of *Tmie* were used to amplify first-strand cDNA prepared from adult mouse cochleae, and genomic DNA from C57BL/6J. RT+ and RT− refer to the presence or absence of reverse transcriptase in the first-strand cDNA reactions. The predicted 768 bp product was detected in cochlear cDNA. NT, no template. Sizes of molecular standards are indicated on the left, in kb.

with the stereocilia pathology found in spinner mice, and would predict a localization of the protein at the apical surface of the hair cell. Immunocytochemical studies with antibodies specific for TMIE will help to distinguish the site of action of the protein and its potential functional roles.

Further characterization of the impact of *Tmie* mutations in the inner ears of spinner mice will provide insight into pathways that are critical for normal maturation of sensory cell function. Analysis of spinner will also help to define the molecular mechanism of hearing loss in humans with defects at the DFNB6 locus, and will provide a system in which to investigate potential therapies that rescue sensory cells and preserve auditory function.

MATERIALS AND METHODS

Mice and genetic mapping

C57BL/6J-+/*sr* heterozygous mice were obtained from the frozen embryo repository at The Jackson Laboratory (Bar Harbor, ME, USA). The original *sr* mutation arose on C57BL/How (8), and has been maintained on a C57BL/6J background by mating homozygous C57BL/6J-*sr/sr* mice to C57BL/6J-+/*sr* heterozygotes. Homozygous *sr/sr* mice were mated with *M. musculus castaneus* (strain CAST/Ei) to produce a (C57BL/6J-*sr* × CAST) F1 generation. F1 mice were intercrossed to produce an F2 generation. The new sr^J allele arose spontaneously in a colony of BXA-4 recombinant inbred mice at The Jackson Laboratory, and was maintained by similar homozygote × heterozygote matings. All mice were maintained in accordance with institutional UCUCA standards.

Genetic markers and genotype analysis

F2 offspring from (C57BL/6J-*sr* × CAST) F1 intercrosses were typed with SSLP (simple sequence length polymorphism) markers from distal chromosome 9 (41). DNA was prepared from tail biopsies of F2 mice as described (42). Affected *sr/sr* F2 mice were identified at weaning age by their circling and hyperactive behaviors, and lack of a startle reflex in response to loud noise. Animals with ambiguous behavior were subjected to a swimming test; *sr/sr* animals are completely unable to remain above the surface of the water. Unaffected mice with recombination events in the critical region were retested to confirm their unaffected status. Genotypes at spinner were inferred from the genotype of flanking markers, or determined by test crosses with *sr/sr* mice. The first 60 F2 mice generated were typed for all markers. An additional 670 F2 mice were first typed with D9Mit212 and D9Mit149; mice that exhibited recombination events within this 4 cM region were then typed with additional markers. Genotype data were analyzed using Map Manager software (43). The most likely gene order was determined by minimizing the total number of crossovers in the region. PCR primers specific for D9Mit markers were obtained from

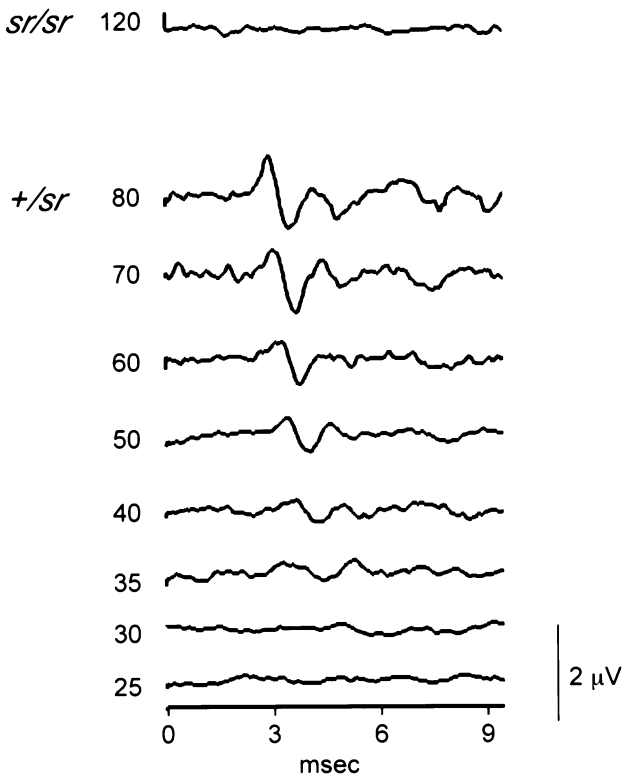

Figure 8. Homozygous spinner mice lack detectable auditory brainstem responses (ABR). Responses to pure tone stimuli of 1, 8 and 24 kHz were measured for two heterozygous +/*sr* and two homozygous *sr/sr* mice at each of three time points (P14, P25 and P90). No responses were detected at any frequency in *sr/sr* mice at any age. Representative recordings from an *sr/sr* mouse (P14) for 8 kHz stimuli at 120 dB SPL and from a +/*sr* mouse (P14) for 8 kHz stimuli at multiple intensities (in dB SPL) are shown.

Research Genetics (Huntsville, AL, USA). All other primers were synthesized at the University of Michigan Oligonucleotide Facility. Two D9Mit markers served as surrogate markers for genes based on close physical association: D9Mit37 (*Mylc*) and D9Mit38 (*Ltf*). *Cdc25a* was localized using an SSLP primer set (5′-CACCCTGCCGTTACACTCTTCTG-3′, 5′-GCACTTGGCGGCTTTTCTCT-3′; C57BL/6J allele size 185 bp; CAST/Ei allele size 192 bp). PCR for analysis of SSLP markers was carried out under standard conditions; products were resolved on 4% agarose gels and visualized with ethidium bromide fluorescence. For analysis of gene-based markers, single-strand conformational polymorphism (SSCP) analysis was performed with end-labeled primers using standard protocols (44). Reaction products were separated on gels composed of 0.4 × MDE (Bio Whittaker, Walkersville, MD, USA)/8% glycerol, using 0.7 × TBE as running buffer and electrophoresis under constant power conditions (10 W) for 12–24 h. Gels were vacuum dried at 70°C, and then exposed to X-ray film (X-Omat AR, Kodak). SSCP primer sets: *Pthr1* (5′-TGTTGCAGGAAGAATGGGAA ACAGTC-3′; 5′-CCTTGAGCACAACACAGGAAGCCAC-3′); *Stac* (5′-TTTGGCTGGCAGGATTGTTCTTTCTTTCTC-3′; 5′-CTTCCTTGTCCCCACTCCCGCTTC-3′); *Tdgf1* (5′-TTTGTCTTGCTTGAACCTTGTCAGTAAC-3′, 5′-TGAGTCGGATGCCCAGAACCA-3′). For localization of the sr^J mutation, we performed a genome-wide linkage screen, comparing MIT marker genotypes of F1 DNA with genotypes of pooled DNA from 20 affected F2 mice. Following discovery of linkage to Chromosome 9, 56 individual affected F2 mice (112 meioses) were typed for additional markers on Chromosome 9.

Physical map construction and characterization of the spinner deletion

Hybridization probes were derived from STS markers non-recombinant and flanking the spinner candidate region and pooled to screen the RPCI-23 BAC genomic library (45). DNA from positively hybridizing BACs was purified using standard methods, and insert overlap was evaluated by PCR and/or hybridization with STS and BAC end markers. BAC inserts were sized by pulsed-field gel electrophoresis. The status of markers on the spinner chromosome was determined by PCR and/or hybridization of *sr/sr* genomic DNA. Marker STS primers were designed from genomic sequence of BAC RP23-79H19 (AC079643): *Pthr1* (5′-CACTCCAGCCCT GCCAGCACGATA-3′; 5′-TCCTCCTCCCACCCTGAA CCCACT-3′); *79H19A* (5′-CAGGGCGGGACATGCT TACAA-3′; 5′-GGGGATGCTGGGAGTCTGGTC-3′); *79H19B* (5′-TGAGGGGCTTTA ACATCAGTAGAGACAT-3′; 5′-CCATAAAGAAGA AACAATAGCAGCAACAAT-3′); *79H19C* (5′-ATCCCC TATCTCACCCCCACATC-3′; 5′-CATCTAGCAATCCCGA GAACCAGTC-3′); *79H19D* (5′-TTTAG ATGGCCACAGGACAATAGC-3′; 5′-CCCCAGG AAAT CACATCACCA-3′); *79H19E* (5′-CAGCC CGCAGT GGAGTGACC-3′; 5′-TGTGATGGGGCAG AATGGAGACC-3′); *195G15-T7* (5′-GTAGT CCGCGCTGGTGCCCTG-3′; 5′-CCTCAAA CTCCTCTCCCCGTCCAG-3′); *Tdgf1* (5′-TGGGCAT CCGACTCAGGTTGTAAAG-3′; 5′-CACGGC CACGCTCGGAATAAA-3′); *Ltf* (5′-GGCAAGGCCAGT TCAGATACAAAGATG-3′; 5′-CACACCCACCGGAAG CAATAAATG-3′).

In order to precisely define the extent of the spinner deletion, we used inverse PCR to amplify genomic DNA from *sr/sr* mice with nested primer sets designed from sequence telomeric to the deletion (primary primer set—5′-GCCCAGCT CCCAATGCACACTCAGA-3′; 5′-CTCTCCCAGC ACGTGCAGAAATAC-3′; secondary primer set: 5′-TGTCC AAAGGCAGGGGTGAGAGC-3′; 5′-TCAGGGG ACCGAGATAAGCCATAGG-3′). Template was prepared by digestion of *sr/sr* genomic DNA with Tsp509I, followed by ligation at a DNA concentration of 1 mg/ml. Amplification conditions: 97°C, 3 min; 35 cycles of 94°C, 30 s; 65°C, 30 s; 72°C, 60 s; final extension of 5 min at 72°C. The sequence of inverse PCR products was compared to genomic sequence in the region AC079643. Based upon this analysis, primer sets were designed to amplify across the centromeric and telomeric breakpoints in normal genomic DNA (centromeric breakpoint set—primer 1: 5′-CCAGTTACGTCAGATCCTACACC-3′; primer 2: 5′-CACAATCCTGACAGCCAAACCTT-3′; telomeric breakpoint set—primer 3: 5′-CTGCCCCTGA GGAGCTCTATGG-3′; primer 4: 5′-CACAACCGCT GGGCACTCTCAT-3′). For Southern analysis, probes were prepared by PCR amplification of BAC RP23-133F23 with primer sets designed from DNA centromeric to the deletion

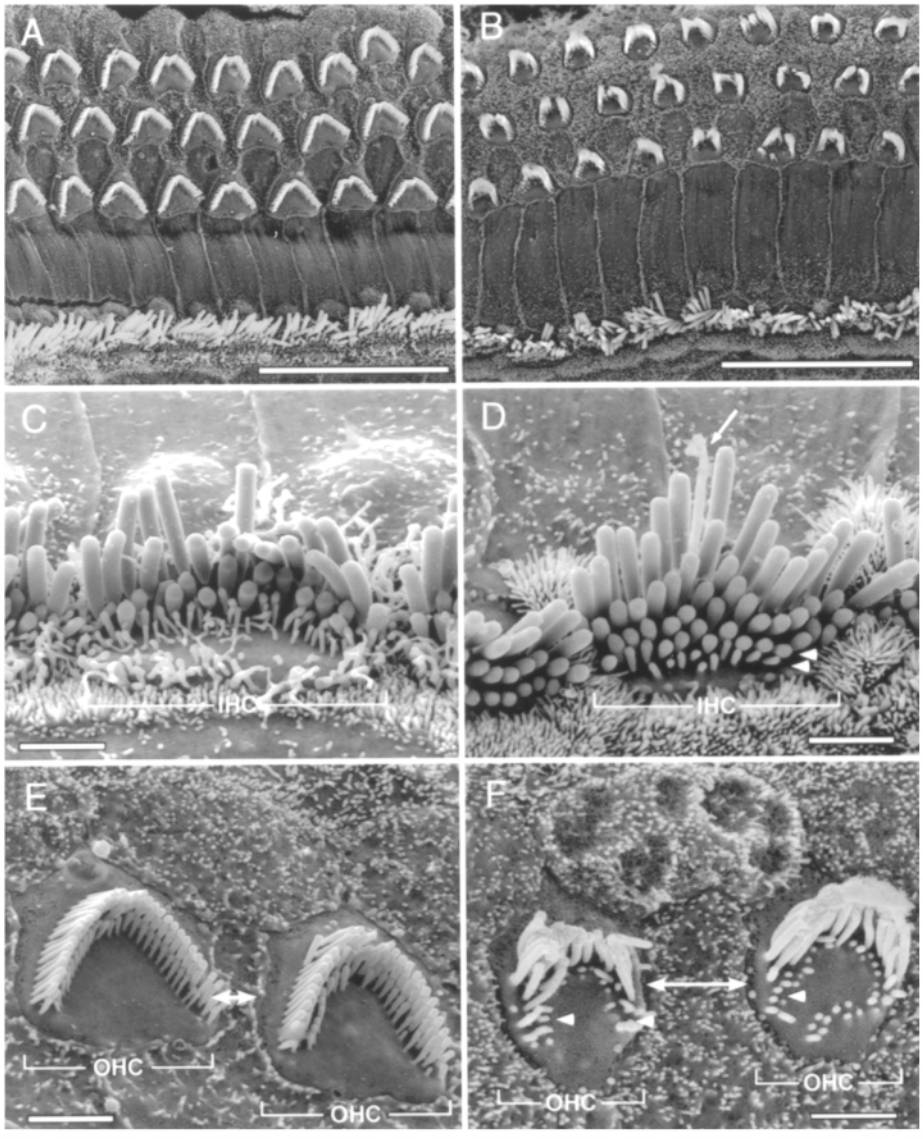

Figure 9. Homozygous spinner mice exhibit sensory hair cell defects during postnatal maturation of the cochlea. (**A**) Sensory neuroepithelium from a control +/*sr* cochlea at P15 exhibited a normal, highly organized pattern of sensory and supporting cells. At the bottom, inner hair cells (IHCs) form a single row of cells with microvilli-like projections (stereocilia) from their apical surfaces. At the top, three rows of outer hair cells (OHCs) are visible. Each OHC possesses a 'V-shaped' stereocilia bundle. (**B**) Sensory neuroepithelium from an *sr/sr* cochlea at P15. Although general neuroepithelial cell patterning was relatively normal, stereocilia bundles on IHCs and OHCs were irregular. (**C**) IHC from a +/*sr* cochlea lacked kinocilia, and exhibited typical bundle characteristics, including three rows of maturing stereocilia. (**D**) IHC from an *sr/sr* cochlea retained single kinocilia (arrow) and exhibited extra rows of developing supernumerary stereocilia (arrowheads). (**E**) OHCs from a +/*sr* cochlea exhibited well-organized, V-shaped stereocilia bundles, and distances between OHCs were normal (double-arrowed line). (**F**) Portions of each stereocilia bundle on OHCs from an *sr/sr* cochlea were missing or shortened (arrowheads), and supernumerary stereocilia were present. The apical surface areas of the OHCs were also decreased compared to +/*sr* OHCs, while the surface areas of supporting cells that surround OHCs in *sr/sr* were correspondingly increased (double-arrowed line). Cochleae from P15 littermates (two +/*sr* and two *sr/sr* mice) were dissected and processed for SEM. All images depict sensory cells from equivalent positions in the lower apex portion of the cochlea. The scale bars in (A) and (B) represent 20 μm; the scale bars in (C)–(F) represent 2 μm.

(probe I: 5′-CCAGTTACGTCAGATCCTACAC-3′; 5′-TAAAACAAAACAAGTGAAGCAAAAGTCTCC-3′; 361 bp product), within the deletion (probe II: 195G15-T7 forward and reverse primers, see above; 446 bp product), and telomeric to the deletion (probe III: 5′-GTGCCC AGCGGTTGTGGTATGTGAC-3′; 5′-GTCTTCCCC AACTCCCCCTCCTCAG-3′; 594 bp product). Genomic DNA from C57BL/6J, C57BL/6J-+/*sr*, and C57BL/6J-*sr/sr* mice was digested with *Bgl*II, electrophoresed in triplicate (5 mg/lane) on a 0.8% agarose gel, and transferred to Zetaprobe GT using standard techniques. Each of the triplicate filters was hybridized with one of the above probes. Hybridization was performed at 65°C in nylon buffer (0.5 M Na_2PO_4; 7% Sodium dodecyl sulfate (SDS); 1 mM EDTA) using an α-[^{32}P]-dATP random labeled PCR product. Final washes were in 0.2× Sodium chloride/sodium citrate (SSC)/0.1% SDS at 65°C. The washed filter was exposed to BioMax film (Kodak) at −80°C.

Gene identification, cDNA sequence assembly, and mutation analysis

The exon content of genomic sequence from BAC RP23-79H19 (AC079643) was evaluated by Genscan analysis (46) and by sequence similarity searches of public databases, including human genome assemblies (47), using the BLAST algorithm (48). Predicted exons were verified by sequence analysis of kidney cDNA clones (IMAGE:1431993 and IMAGE:1432228) and by RT–PCR with gene-specific primer sets. Additional cDNA sequences were identified by 5′ and 3′ RACE from brain and kidney Marathon cDNA (Clontech, Palo Alto, CA, USA). Total RNA was isolated from adult mouse brain using Trizol reagent (Invitrogen, Carlstad, CA, USA). Poly(A)$^+$ transcripts were purified using PolyATract (Promega, Madison, WI, USA); first-strand cDNA synthesis was performed on 5 mg poly(A)$^+$ RNA using oligo-dT primers with the Superscript II system (Invitrogen). For mutation detection in *sr*^{J} and control strains, overlapping RT–PCR products were amplified using gene-specific primer sets, and products were gel purified and sequenced as described previously (49). For confirmation of the nonsense mutation identified in *sr*^{J}, we amplified genomic DNA (100 ng) from *sr*^{J}/*sr*^{J} and BXA-4 mice with primers that flank exon 5 of *Tmie* (5′-CTGTGAGACAAGCTTAAGCAGATGGAGT-3′; 5′-CAATTGGAACAGTGGGAGTGAGGAA-3′), and sequenced the gel-purified products. Domain structure of the conceptual TMIE protein sequence was evaluated using SignalP (50) and TMHMM (19).

Expression analysis

A northern blot containing RNA isolated from adult mouse tissues (Stratagene, La Jolla, CA, USA) was hybridized with a probe derived from the 3′ UTR of *Tmie* (probe II, above). Hybridization was performed as described above for Southern analysis. The filter was stripped by two 15 min incubations in 0.1× SSC/1% SDS at 95°C, and then rehybridized with a human β-actin probe at 60°C. RNA was prepared from adult mouse cochleae using the SV Total RNA Isolation System (Promega). RT–PCR of cochlear RNA was performed with primers designed to amplify across exons 3–6 of *Tmie* (5′-GTGTCGCCACGCAGCT GGTA-3′; 5′-GACAACCTGTTCAGT CTTGCCATCCTA-3′).

Scanning electron microscopy

Deeply anesthetized mice derived from a C57BL/6J-+/*sr* × C57BL/6J-*sr/sr* cross were decapitated and cochlea obtained and fixed in 2% glutaraldehyde. Four *sr/sr* and four +/*sr* mice at P14 were analyzed. Tissues were prepared for SEM analysis as previously described (32). Samples were analyzed using a Philips XL30 FEG scanning electron microscope.

Electrophysiological analysis

Auditory brainstem analysis was performed on mice from the CAST/Ei intercross, using pure tone stimuli of 1, 8 and 24 kHz, as previously described (29). Two *sr/sr* mice and two +/*sr* mice from each of three time points (P14, P25 and P90) were analyzed.

ACKNOWLEDGEMENTS

We thank Margaret Lomax, Hana Odeh, Didi Robins, Sally Camper and Miriam Meisler for critical reading of the manuscript. We are also grateful to Tzy-Wen Gong for generous assistance with preparation of mouse cochlear RNA. This work was supported by grants from the National Organization for Hearing Research (DCK), the American Hearing Research Foundation (DCK), NIH-NIDCD grants DC04410 (DCK), DC02982 (DCK, DFD, and YR) and NIH-NIDCD contract DC62108 (KRJ).

REFERENCES

1. Morton, N.E. (1991) Genetic epidemiology of hearing impairment. *Ann. N. Y. Acad. Sci.*, **630**, 16–31.
2. Mehl, A.L. and Thomson, V. (1998) Newborn hearing screening: the great omission. *Pediatrics*, **101**, E4.
3. Petit, C., Levilliers, J. and Hardelin, J.P. (2001) Molecular genetics of hearing loss. *Annu. Rev. Genet.*, **35**, 589–646.
4. Resendes, B.L., Williamson, R.E. and Morton, C.C. (2001) At the speed of sound: gene discovery in the auditory system. *Am. J. Hum. Genet.*, **69**, 923–935.
5. Keats, B.J. and Berlin, C.I. (1999) Genomics and hearing impairment. *Genome Res.*, **9**, 7–16.
6. Probst, F.J. and Camper, S.A. (1999) The role of mouse mutants in the identification of human hereditary hearing loss genes. *Hear. Res.*, **130**, 1–6.
7. Steel, K.P. and Kros, C.J. (2001) A genetic approach to understanding auditory function. *Nat. Genet.*, **27**, 143–149.
8. Deol, M.S. and Robins, M.W. (1962) The spinner mouse. *J. Heredity*, **53**, 133–136.
9. Fox, S., Eicher, E.M. and Reynolds, S. (1978) *sr. Mouse News Lett.*, **58**, 50.
10. DeBry, R.W. and Seldin, M.F. (1996) Human/mouse homology relationships. *Genomics*, **33**, 337–351.
11. Fukushima, K., Ramesh, A., Srisailapathy, C.R., Ni, L., Wayne, S., O'Neill, M.E., Van Camp, G., Coucke, P., Jain, P., Wilcox, E.R. *et al.* (1995) An autosomal recessive nonsyndromic form of sensorineural hearing loss maps to 3p-DFNB6. *Genome Res.*, **5**, 305–308.
12. Steel, K.P. and Bock, G.R. (1983) Hereditary inner-ear abnormalities in animals. Relationships with human abnormalities. *Arch. Otolaryngol.*, **109**, 22–29.
13. Saccone, S., Rapisarda, A., Motta, S., Dono, R., Persico, G.M. and Della Valle, G. (1995) Regional localization of the human EGF-like growth factor CRIPTO gene (TDGF-1) to chromosome 3p21. *Hum. Genet.*, **95**, 229–230.
14. Demetrick, D.J. and Beach, D.H. (1993) Chromosome mapping of human CDC25A and CDC25B phosphatases. *Genomics*, **18**, 144–147.
15. Cohen-Haguenauer, O., Barton, P.J., Van Cong, N., Cohen, A., Masset, M., Buckingham, M. and Frezal, J. (1989) Chromosomal assignment of two myosin alkali light-chain genes encoding the ventricular/slow skeletal muscle isoform and the atrial/fetal muscle isoform (MYL3, MYL4). *Hum. Genet.*, **81**, 278–282.
16. Pausova, Z., Bourdon, J., Clayton, D., Mattei, M.G., Seldin, M.F., Janicic, N., Riviere, M., Szpirer, J., Levan, G., Szpirer, C. *et al.* (1994) Cloning of a parathyroid hormone/parathyroid hormone-related peptide receptor (PTHR) cDNA from a rat osteosarcoma (UMR 106) cell line: chromosomal assignment of the gene in the human, mouse, and rat genomes. *Genomics*, **20**, 20–26.
17. Kawai, J., Suzuki, H., Hara, A., Hirose, K. and Watanabe, S. (1998) Human and mouse chromosomal mapping of Stac, a neuron-specific protein with an SH3 domain. *Genomics*, **47**, 140–142.
18. Soisson, S.M., Nimnual, A.S., Uy, M., Bar-Sagi, D. and Kuriyan, J. (1998) Crystal structure of the Dbl and pleckstrin homology domains from the human Son of sevenless protein. *Cell*, **95**, 259–268.

19. Krogh, A., Larsson, B., von Heijne, G. and Sonnhammer, E.L. (2001) Predicting transmembrane protein topology with a hidden Markov model: application to complete genomes. *J. Mol. Biol.*, **305**, 567–580.
20. Pickles, J.O. and Corey, D.P. (1992) Mechanoelectrical transduction by hair cells. *Trends Neurosci.*, **15**, 254–259.
21. Lim, D.J. and Anniko, M. (1985) Developmental morphology of the mouse inner ear. A scanning electron microscopic observation. *Acta Otolaryngol. Suppl. (Stockh)*, **422**, 1–69.
22. Naz, S., Giguere, C.M., Kohrman, D.C., Mitchem, K.L., Riazuddin, S., Morell, R.J., Ramesh, A., Srisailpathy, S., Deshmukh, D., Riazuddin, S. *et al.* (2002) Mutations in a novel gene TMIE are associated with hearing loss at the DFNB6 locus. *Am. J. Hum. Genet.*, in press.
23. Self, T., Mahony, M., Fleming, J., Walsh, J., Brown, S.D. and Steel, K.P. (1998) Shaker-1 mutations reveal roles for myosin VIIA in both development and function of cochlear hair cells. *Development*, **125**, 557–566.
24. Self, T., Sobe, T., Copeland, N.G., Jenkins, N.A., Avraham, K.B. and Steel, K.P. (1999) Role of myosin VI in the differentiation of cochlear hair cells. *Dev. Biol.*, **214**, 331–341.
25. Probst, F.J., Fridell, R.A., Raphael, Y., Saunders, T.L., Wang, A., Liang, Y., Morell, R.J., Touchman, J.W., Lyons, R.H., Noben-Trauth, K. *et al.* (1998) Correction of deafness in shaker-2 mice by an unconventional myosin in a BAC transgene. *Science*, **280**, 1444–1447.
26. Di Palma, F., Holme, R.H., Bryda, E.C., Belyantseva, I.A., Pellegrino, R., Kachar, B., Steel, K.P. and Noben-Trauth, K. (2001) Mutations in Cdh23, encoding a new type of cadherin, cause stereocilia disorganization in waltzer, the mouse model for Usher syndrome type 1D. *Nat. Genet.*, **27**, 103–107.
27. Alagramam, K.N., Murcia, C.L., Kwon, H.Y., Pawlowski, K.S., Wright, C.G. and Woychik, R.P. (2001) The mouse Ames waltzer hearing-loss mutant is caused by mutation of Pcdh15, a novel protocadherin gene. *Nat. Genet.*, **27**, 99–102.
28. Alagramam, K.N., Zahorsky-Reeves, J., Wright, C.G., Pawlowski, K.S., Erway, L.C., Stubbs, L. and Woychik, R.P. (2000) Neuroepithelial defects of the inner ear in a new allele of the mouse mutation Ames waltzer. *Hear. Res.*, **148**, 181–191.
29. Raphael, Y., Kobayashi, K.N., Dootz, G.A., Beyer, L.A., Dolan, D.F. and Burmeister, M. (2001) Severe vestibular and auditory impairment in three alleles of Ames waltzer (av) mice. *Hear. Res.*, **151**, 237–249.
30. Littlewood Evans, A. and Muller, U. (2000) Stereocilia defects in the sensory hair cells of the inner ear in mice deficient in integrin alpha8beta1. *Nat. Genet.*, **24**, 424–428.
31. Zheng, L., Sekerkova, G., Vranich, K., Tilney, L.G., Mugnaini, E. and Bartles, J.R. (2000) The deaf jerker mouse has a mutation in the gene encoding the espin actin-bundling proteins of hair cell stereocilia and lacks espins. *Cell*, **102**, 377–385.
32. Beyer, L.A., Odeh, H., Probst, F.J., Lambert, E.H., Dolan, D.F., Camper, S.A., Kohrman, D.C. and Raphael, Y. (2000) Hair cells in the inner ear of the pirouette and shaker 2 mutant mice. *J. Neurocytol.*, **29**, 227–240.
33. Spoendlin, H. (1974) Neuroanatomy of the cochlea. In Zwicker, E. and Terhardt, E. (eds), *Facts and Models in Hearing*. Springer, New York, pp. 18–32.
34. Steel, K.P. and Kros, C.J. (2001) A genetic approach to understanding auditory function. *Nat. Genet.*, **27**, 143–149.
35. Joensuu, T., Hamalainen, R., Yuan, B., Johnson, C., Tegelberg, S., Gasparini, P., Zelante, L., Pirvola, U., Pakarinen, L., Lehesjoki, A.E. *et al.* (2001) Mutations in a novel gene with transmembrane domains underlie Usher syndrome type 3. *Am. J. Hum. Genet.*, **69**, 673–684.
36. Kurima, K., Peters, L.M., Yang, Y., Riazuddin, S., Ahmed, Z.M., Naz, S., Arnaud, D., Drury, S., Mo, J., Makishima, T. *et al.* (2002) Dominant and recessive deafness caused by mutations of a novel gene, TMC1, required for cochlear hair-cell function. *Nat. Genet.*, **30**, 277–284.
37. Vreugde, S., Erven, A., Kros, C.J., Marcotti, W., Fuchs, H., Kurima, K., Wilcox, E.R., Friedman, T.B., Griffith, A.J., Balling, R. *et al.* (2002) Beethoven, a mouse model for dominant, progressive hearing loss DFNA36. *Nat. Genet.*, **30**, 257–258.
38. Tsukita, S. and Yonemura, S. (1999) Cortical actin organization: lessons from ERM (ezrin/radixin/moesin) proteins. *J. Biol. Chem.*, **274**, 34507–34510.
39. Denker, S.P., Huang, D.C., Orlowski, J., Furthmayr, H. and Barber, D.L. (2000) Direct binding of the Na–H exchanger NHE1 to ERM proteins regulates the cortical cytoskeleton and cell shape independently of H(+) translocation. *Mol. Cell*, **6**, 1425–1436.
40. Yonemura, S., Hirao, M., Doi, Y., Takahashi, N., Kondo, T. and Tsukita, S. (1998) Ezrin/radixin/moesin (ERM) proteins bind to a positively charged amino acid cluster in the juxta-membrane cytoplasmic domain of CD44, CD43, and ICAM-2. *J. Cell Biol.*, **140**, 885–895.
41. Dietrich, W.F., Miller, J.C., Steen, R.G., Merchant, M., Damron, D., Nahf, R., Gross, A., Joyce, D.C., Wessel, M., Dredge, R.D. *et al.* (1994) A genetic map of the mouse with 4,006 simple sequence length polymorphisms. *Nat. Genet.*, **7**, 220–245.
42. Ting, C.N., Rosenberg, M.P., Snow, C.M., Samuelson, L.C. and Meisler, M.H. (1992) Endogenous retroviral sequences are required for tissue-specific expression of a human salivary amylase gene. *Genes Dev.*, **6**, 1457–1465.
43. Manly, K.F. (1993) A Macintosh program for storage and analysis of experimental genetic mapping data. *Mamm. Genome*, **4**, 303–313.
44. Beier, D.R. (1993) Single-strand conformation polymorphism (SSCP) analysis as a tool for genetic mapping. *Mamm. Genome*, **4**, 627–631.
45. Osoegawa, K., Tateno, M., Woon, P.Y., Frengen, E., Mammoser, A.G., Catanese, J.J., Hayashizaki, Y. and de Jong, P.J. (2000) Bacterial artificial chromosome libraries for mouse sequencing and functional analysis. *Genome Res.*, **10**, 116–128.
46. Burge, C. and Karlin, S. (1997) Prediction of complete gene structures in human genomic DNA. *J. Mol. Biol.*, **268**, 78–94.
47. Venter, J.C., Adams, M.D., Myers, E.W., Li, P.W., Mural, R.J., Sutton, G.G., Smith, H.O., Yandell, M., Evans, C.A., Holt, R.A. *et al.* (2001) The sequence of the human genome. *Science*, **291**, 1304–1351.
48. Altschul, S.F., Madden, T.L., Schaffer, A.A., Zhang, J., Zhang, Z., Miller, W. and Lipman, D.J. (1997) Gapped BLAST and PSI-BLAST: a new generation of protein database search programs. *Nucleic Acids Res.*, **25**, 3389–3402.
49. Burgess, D.L., Kohrman, D.C., Galt, J., Plummer, N.W., Jones, J.M., Spear, B. and Meisler, M.H. (1995) Mutation of a new sodium channel gene, Scn8a, in the mouse mutant 'motor endplate disease'. *Nat. Genet.*, **10**, 461–465.
50. Nielsen, H., Engelbrecht, J., Brunak, S. and von Heijne, G. (1997) Identification of prokaryotic and eukaryotic signal peptides and prediction of their cleavage sites. *Protein Eng.*, **10**, 1–6.
51. Kozak, M. (1996) Interpreting cDNA sequences: some insights from studies on translation. *Mamm. Genome*, **7**, 563–574.